Expanded dynamic range of fluorescent indicators for Ca^{2+} by circularly permuted yellow fluorescent proteins

Takeharu Nagai*†, Shuichi Yamada‡, Takashi Tominaga§, Michinori Ichikawa§, and Atsushi Miyawaki*¶

*Laboratory for Cell Function and Dynamics, Advanced Technology Development Group, and §Laboratory for Brain-Operative Devices, Brain Science Institute, RIKEN, 2-1 Hirosawa, Wako, Saitama 351-0198, Japan; †Structure and Function of Biomolecules, Precursory Research for Embryonic Science and Technology (PRESTO), Japan Science and Technology Agency (JST), 4-1-8 Hon-cho, Kawaguchi, Saitama 351-0198, Japan; and ‡Laboratory of Signal Transduction, Institute for Virus Research, Kyoto University, Kawaharacho 53, Shogoin, Sakyo-ku, Kyoto 606-8507, Japan

Edited by Roger Y. Tsien, University of California at San Diego, La Jolla, CA, and approved May 19, 2004 (received for review January 29, 2004)

Fluorescence resonance energy transfer (FRET) technology has been used to develop genetically encoded fluorescent indicators for various cellular functions. Although most indicators have cyan- and yellow-emitting fluorescent proteins (CFP and YFP) as FRET donor and acceptor, their poor dynamic range often prevents detection of subtle but significant signals. Here, we optimized the relative orientation of the two chromophores in the Ca^{2+} indicator, yellow cameleon (YC), by fusing YFP at different angles. We generated circularly permuted YFPs (cpYFPs) that showed efficient maturation and acid stability. One of the cpYFPs incorporated in YC absorbs a great amount of excited energy from CFP in its Ca^{2+}-saturated form, thereby increasing the Ca^{2+}-dependent change in the ratio of YFP/CFP by nearly 600%. Both in cultured cells and in the nervous system of transgenic mice, the new YC enables visualization of subcellular Ca^{2+} dynamics with better spatial and temporal resolution than before. Our study provides an important guide for the development and improvement of indicators using GFP-based FRET.

Cameleons are genetically encoded fluorescent indicators for Ca^{2+} based on GFP variants and calmodulin (CaM) (1, 2). They are chimeric proteins composed of a short-wavelength variant of GFP, CaM, a glycylglycine linker, the CaM-binding peptide of myosin light-chain kinase (M13), and a long-wavelength variant of GFP. Ca^{2+} binding to CaM initiates an intramolecular interaction between CaM and M13, which changes the chimeric protein from an extended to a more compact conformation, thereby increasing the efficiency of fluorescence resonance energy transfer (FRET) from the shorter- to the longer-wavelength variant of GFP. Yellow cameleons (YCs) have cyan and yellow fluorescent proteins (CFP and YFP) as the FRET donor and acceptor, respectively. YCs are classified into several groups based on the composition of their Ca^{2+}-sensing domains. For example, YC2 has an intact CaM and thus shows high affinity for Ca^{2+}. On the other hand, YC3 and YC4 are low-affinity indicators because of mutations in the Ca^{2+}-binding loops of their CaM domains. These YCs have been made more resistant to acidification by replacing the original YFP with EYFP.1 (3). The improved YCs include YC2.1 and YC3.1. In addition, some YCs have been made to mature more quickly by using especially bright versions of YFP such as citrine (4) or Venus (5). In this way, YCs have been improved mainly by optimizing the YFP component.

Despite the above-mentioned improvements, YCs still suffer from poor dynamic range. The best versions available currently, such as YC2.12 or YC3.12, exhibit at most a 120% change in the ratio of YFP/CFP upon Ca^{2+} binding *in vitro*. These YCs do not have good signal-to-noise ratios, particularly when they are targeted to organelles or submicroscopic environments, because of low levels of signal. It has been also suggested that their dynamic range is attenuated *in vivo* depending on the abundance of endogenous CaM and CaM-binding proteins that may interact with the sensing domains of YCs.

In the present study, we have attempted to modify the acceptor to increase the dynamic range of the indicator. To achieve a Ca^{2+}-dependent large change in the relative orientation and distance between the fluorophores of CFP and YFP, we assumed that optimization of the length and sequence of the linkers used in YCs would yield only moderate improvement. Thus, we took a more rigorous approach that used a circularly permuted GFP (cpGFP), in which the N and C portions were interchanged and reconnected by a short spacer between the original termini (6, 7). By using cpYFPs that are resistant to acidification and that mature efficiently, we attempted to vary the relative orientation of the two chromophores' transition dipoles.

Materials and Methods

Gene Construction. The cDNAs of the 5′ portions of the cpVenus variants were amplified by PCR using sense primers containing a *Bam*HI site and reverse primers containing the sequence encoding the linker (GGSGG) between the natural N and C termini. The cDNAs of their 3′ portions were extended by PCR at the 5′ end with the sequence encoding the linker and at the 3′ end with the sequence containing an *Eco*RI site. The entire cDNAs of the cpVenus variants were amplified by using a mixture of the two PCR products with the *Bam*HI and *Eco*RI containing primers. The restricted products were cloned in-frame into the *Bam*HI/*Eco*RI sites of $pRSET_B$ (Invitrogen), yielding cp49Venus, cp157Venus, cp173Venus, cp195Venus, and cp229Venus. Then the 5′ end of the cDNA of cp49Venus, cp157Venus, cp173Venus, cp195Venus, or cp229Venus was modified by PCR to have a *Sac*I site; this N-terminal EL (Glu-Leu) sequence encoded by the *Sac*I recognition site was followed in the five variants by a Met residue and then Thr-49, Gln-157, Asp-173, Leu-195, and Ile-229, respectively. The *Sac*I/*Eco*RI fragments were substituted for the gene encoding Venus in YC3.12/$pRSET_B$ to generate YC3.20, YC3.30, YC3.60, YC3.70, and YC3.90, respectively. YC2.60 and YC4.60 were generated from YC3.60 by exchanging the CaM domains. For mammalian expression, the cDNAs of YC3.12 and YC3.60 were subcloned into pcDNA3 (Invitrogen). To localize YC3.60 beneath the plasma membrane, the CAAX box of Ki-Ras was

This paper was submitted directly (Track II) to the PNAS office.

Freely available online through the PNAS open access option.

Abbreviations: FRET, fluorescence resonance energy transfer; CFP, cyan-emitting mutant of GFP; YFP, yellow-emitting mutant of GFP; YC, yellow cameleon; cpGFP, circularly permuted GFP; CaM, calmodulin; $[Ca^{2+}]_c$, cytosolic Ca^{2+} concentration; $[Ca^{2+}]_{pm}$, Ca^{2+} concentrations beneath the plasma membrane; CCD, charge-coupled device; ACSF, artificial cerebrospinal fluid.

Data deposition: The sequences for YC2.60, YC3.60, YC4.60, and $YC3.60_{pm}$ reported in this paper have been deposited in the GenBank database (accession nos. AB178711–AB178714, respectively).

¶To whom correspondence should be addressed. E-mail: matsushi@brain.riken.jp.

www.pnas.org/cgi/doi/10.1073/pnas.0400417101

fused to the C terminus of YC3.60 through a linker sequence (GTGGSGGGTGGSGGGT). For transgenic mice construction, $YC3.60_{pm}$ cDNA was subcloned into the *Eco*RI site of the pCAGGS expression vector, which contains the β-actin promoter, cytomegalovirus enhancer, β-actin intron, and bovine globin polyadenylation signal (8). A *Bam*HI-*Sal*I fragment containing the promoter/enhancer and coding sequence was prepared for injection into BCF1 × BCF1 fertilized eggs.

Protein Expression, *in Vitro* Spectroscopy, Ca^{2+}, and pH Titrations. Recombinant YC proteins with N-terminal polyhistidine tags were expressed in *Escherichia coli* [JM109(DE3)] at room temperature, purified, and spectroscopically characterized as described (1). Steady-state fluorescence polarization was measured by using BEACON (Takara Bio Inc., Otsu, Japan) and using a 440DF20 excitation filter and a 535DF25 emission filter. Ca^{2+} titrations were performed by reciprocal dilution of Ca^{2+}-free and Ca^{2+}-saturated buffers prepared by using *O*,*O*′bis(2-aminoethyl)ethyleneglycol-*N*,*N*,*N*′,*N*′tetraacetic acid (EGTA), *N*-(2-hydroxyethyl)ethylenediamine-*N*,*N*′,*N*′-triacetic acid (HEEDTA), or nitrilotriacetic acid (NTA). pH titrations were performed by using a series of buffers prepared with pH values ranging from 5.8 to 8.4 as described (3).

Cell Culture and Transfection. HeLa cells were grown in Dulbecco's modified Eagle's medium containing 10% heat-inactivated FCS. Cells were transfected with expression vectors encoding YC3.60 or YC3.12 by using SuperFect (Qiagen, Valencia, CA).

Production of Transgenic Mice. The incorporation of the transgene into the genome was detected in 10 lines by PCR analysis. Among them, line no. 62 produced bright fluorescence in the brain and was used.

Slice Preparation. Hippocampal slices were prepared from 15-day-old F_1 animals. The brains were quickly cooled in iced artificial cerebrospinal fluid [ACSF, which contained 124 mM NaCl, 2.5 mM KCl, 2 mM $CaCl_2$, 2 mM $MgSO_4$, 1.25 mM NaH_2PO_4, 26 mM $NaHCO_3$, and 10 mM glucose (pH 7.4) after bubbling with mixed 95% O_2/5% CO_2 gas]. After cooling for 5 min, the hippocampus was dissected out along with the surrounding cortex and sliced into 400-μm-thick sections with a vibratome (Leica, Deerfield, IL). Each slice was transferred onto a fine-mesh membrane filter (Omni Pore membrane filter, JHWP01300, Millipore) held in place by a thin Plexiglas ring after a short incubation in 95% O_2/5% CO_2 gas mixture.

Imaging. Between 2 and 4 days after transfection, HeLa cells in Hanks' balanced salt solution buffer (GIBCO) were subjected to imaging. Wide-field fluorescence observations were performed on an IX-70 inverted microscope by using a UApo 40×, 1.35 numerical aperture (NA), oil-immersion objective (Olympus). Dual-emission imaging with YCs used a 440DF20 excitation filter, a 455DRLP dichroic mirror, and two emission filters (480DF30 for CFP and 535DF25 for YFP) alternated by using a filter changer (Lambda 10-2, Sutter Instruments, Novato, CA). Interference filters were obtained from Omega Optical (Brattleboro, VT). Fluorescence emission from YCs was imaged by using a cooled charge-coupled device (CCD) camera (Cool SNAP fx, Roper Scientific, Duluth, GA). Image acquisition and analysis were performed by using METAMORPH/METAFLUOR 5.0 software (Universal Imaging, Media, PA). Video rate confocal FRET images were acquired by using an IX-71 equipped with a PlanApo 60×, 1.4 NA, oil-immersion objective (Olympus), a spinning disk-type confocal unit (CSU21, Yokogawa, Tokyo), a diode-pumped solid state laser (430 nm) (Melles Griot), and a 3CCD color camera (ORCA-3CCD, Hamamatsu Photonics, Hamamatsu City, Japan). Image acquisition and analysis were performed by using AQUACOSMOS/ASHURA software (Hamamatsu Photonics). For imaging hippocampal slice, a slice supported by the Plexiglas ring was transferred to an immersion-type recording chamber. Slices were continuously perfused with ACSF without Mg^{2+} at a rate of 1 ml/min. The ACSF was continuously bubbled with a 95% O_2/5% CO_2 gas mixture and warmed to 31°C before being channeled to the recording chamber. Wide-field emission from YFP was collected at 100 Hz by a high-speed CCD camera (MiCAM01, Brainvison, Tokyo) and a BX-50 upright microscope with a 2×, 0.2 NA, objective (Olympus), a 420DF40 excitation filter, a 505DRLP-XR dichroic mirror, and a 460LP emission filter. The ratio of the fractional change in fluorescence of $YC3.60_{pm}$ to the initial, prestimulation amount of fluorescence ($\Delta F/F_0$) was calculated and used as the optical signal. The analyses of the optical signals were done with a procedure developed for Igor Pro (WaveMetrics, Lake Oswego, OR). A glass microcapillary tube (5 μm outer diameter, filled with ACSF) was used as a monopolar stimulating electrode and a recording electrode for field potential recordings. Three hundred milliseconds after the starting of image collection, the stimulus, repeated 30 times for 0.5 ms at 10-ms intervals, was applied to the Schaffer collateral pathway.

Results

Circular permutation was conducted on Venus by using a peptapeptide linker GGSGG to connect the natural N and C

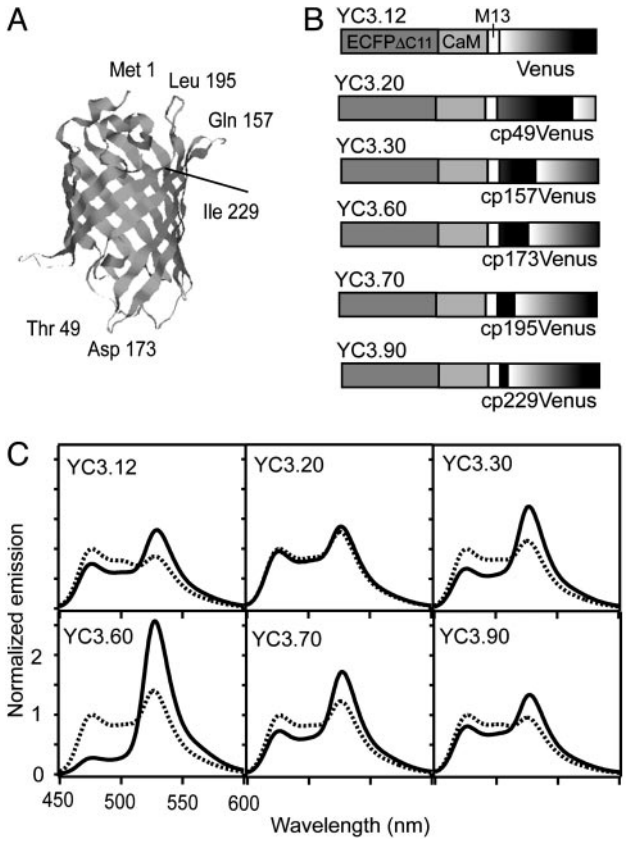

Fig. 1. Schematic structures and spectral properties of YC3.12 and the new YC variants. (*A*) The three-dimensional structure of GFP with the positions of the original (Met-1) and new N termini (Thr-49, Gln-157, Asp-173, Leu-195, and Ile-229) are indicated. (*B*) Domain structures of YC3.12, YC3.20, YC3.30, YC3.60, YC3.70, and YC3.90. XCaM, *Xenopus* CaM; E104Q, mutation of the conserved bidentate glutamate (E104) at position 12 of the third Ca^{2+} binding loop to glutamine. (*C*) Emission spectra of YC variants (excitation at 435 nm) at zero (dotted line) and saturated Ca^{2+} (solid line).

Table 1. Ca^{2+} responses of the conventional and new YC variants

	R_{min}	R_{max}	Dynamic range, %	Anisotropy $-Ca^{2+}$	Anisotropy $+Ca^{2+}$
YC3.12	0.9	1.8	100	0.23	0.17
YC3.20	1.3	1.4	10	0.06	0.10
YC3.30	1.1	2.6	140	0.16	0.07
YC3.60	1.4	9.3	560	0.12	−0.05
YC3.70	1.2	2.4	100	0.15	0.09
YC3.90	1.0	1.7	70	0.17	0.10

Table 2. Affinities for Ca^{2+} of YC3.60 and its derivatives

	K'_d, nM	Fraction, %	Hill coefficient
YC2.60	40	—	2.4
YC3.60	250	—	1.7
YC4.60	58	41	1.7
	14,400	59	0.9

K'_d, apparent dissociation constant.

termini. New termini were introduced into surface-exposed loop regions of the β-barrel. cp49Venus, cp157Venus, cp173Venus, cp195Venus, and cp229Venus were given new N termini at Thr-49, Gln-157, Asp-173, Leu-195, and Ile-229, respectively. When expressed in bacteria and mammalian cultured cells, they matured efficiently and were resistant to acidification to a similar extent to their parent protein Venus. The use of these cpVenus proteins in addition to Venus would create significant variation in the relative spatial orientation of YFP within the YC complex because Met-1, Thr-49, Gln-157, Leu-195, and Ile-229 reside at different sites on the β-barrel; Thr-49 and Asp-173 are particularly far removed, at the opposite end of the β-barrel from the other residues (Fig. 1*A*).

As a parent YC, YC3.12 (5) was used initially because of its monophasic Ca^{2+} sensitivity (1); it has a mutation of a conserved glutamate (E104) in the third Ca^{2+}-binding site of CaM and belongs to the YC3 group. We replaced Venus in YC3.12 with cp49Venus, cp157Venus, cp173Venus, cp195Venus, and cp229Venus to generate YC3.20, YC3.30, YC3.60, YC3.70, and YC3.90, respectively (Fig. 1*B*). All of these new YCs were expressed efficiently and folded in bacteria, similar to YC3.12. Next, their Ca^{2+} sensitivity was examined by *in vitro* experiments. Remarkably, YC3.60 gave a severalfold increase in the emission ratio of YFP to CFP between zero and saturating Ca^{2+} concentrations whereas YC3.30, YC3.70, and YC3.90 showed a similar dynamic range to that of YC3.12; YC3.20 showed only a slight response to Ca^{2+} (Fig. 1*C*). Although the substitution of cp173Venus for Venus generally favored the FRET from CFP, this effect was much more striking in the complex's Ca^{2+}-saturated form [R_{max}: 1.8 (YC3.12) vs. 9.3 (YC3.60)] than in its Ca^{2+}-depleted form [R_{min}: 0.87 (YC3.12) vs. 1.4 (YC3.60)] (Table 1). To examine the relative angle between the chromophores of CFP and YFP, steady-state polarization was measured with excitation of CFP at 440 nm and emission of YFP at 535 nm. On the whole, the Ca^{2+}-dependent decrease in anisotropy correlated with the increase in the emission ratio of YFP to CFP, except for YC3.20, which showed a Ca^{2+}-dependent increase in anisotropy (Fig. 2*A*).

The emission ratio (530:480) of YC3.60 showed a monophasic Ca^{2+}-dependency with an apparent dissociation constant (K'_d) of 0.25 μM and a Hill constant (n) of 1.7 (Fig. 2*B*, circles). To change the Ca^{2+} affinity of YC3.60, we replaced the mutated CaM with either WT CaM or a CaM containing a mutation in the first Ca^{2+}-binding loop (E31Q) (1). The resulting YCs belong to the YC2 and YC4 groups and are called YC2.60 and YC4.60, respectively. YC2.60 showed a nearly monophasic response (K'_d, 40 nM; n, 2.4); there was a tiny depression on the titration curve at 0.2–0.3 μM (Fig. 2*B*, triangles), reminiscent of the biphasic Ca^{2+}-sensitivity of the original CaM-M13 hybrid protein (1, 9). As described (1), E31Q in YC4.60 gave a significantly lower Ca^{2+} affinity with a clear biphasic response (K'_d, 58 nM; n, 1.7; K'_d, 14.4 μM; n, 0.9) (Fig. 2*B*, squares). The high dynamic range achieved in YC3.60 (560%) was preserved in YC2.60, but slightly attenuated in YC4.60 (dynamic range, 360%). The high- and low-affinity components of YC4.60 contributed to 41% and 59% of the response. Because the cpVenus proteins displayed similar acid sensitivity (pK_a, 6.0) to EYFP-V68L/Q69K (EYFP.1) or Venus (results not shown), YC3.60 was expected to be as pH-resistant as YC3.1 and YC3.12. The pH titration curves in Fig. 2*C* show that the YFP/CFP ratio does not change significantly in the presence and absence of Ca^{2+} over a physiological range of pH, from 6.5 to 8.2. Compared with YC3.1 and YC3.12, however, YC3.60 gives a large Ca^{2+}-dependent response that overwhelms the noise due to the pH change, resulting in a much better signal-to-noise ratio. The properties of YC variants are summarized in Tables 1 and 2.

The superiority of YC3.60 to YC3.12 was demonstrated clearly in experiments in which we monitored cytosolic free Ca^{2+} concentrations ($[Ca^{2+}]_c$) in HeLa cells. HeLa cells transfected with the same amount of cDNAs encoding either YC3.60 or YC3.12 produced equally bright fluorescence signals in the cytosolic compartment. Fig. 3 *A* and *B* show the time courses of the spatially averaged YFP/CFP ratios from HeLa cells expressing YC3.60 and YC3.12, respectively. YC3.60 clearly gives a much larger responses to a supramaximal dose of ATP (30 μM) and nearly 6-fold-larger ratios of R_{max} to R_{min} than does YC3.12.

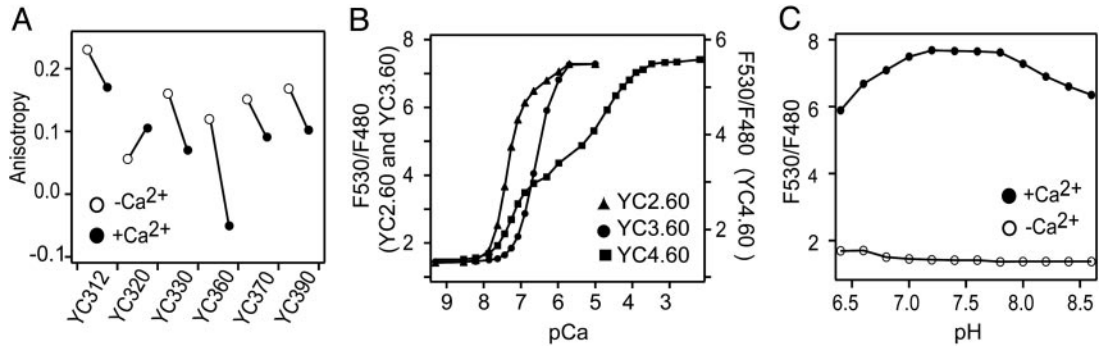

Fig. 2. Properties of YC variants *in vitro*. (*A*) Fluorescence anisotropy of YC variants (YC3.12, YC3.20, YC3.30, YC3.60, YC3.70, and YC3.900) at zero and saturated Ca^{2+}. (*B*) Ca^{2+} titration curves of YC2.60 (triangles), YC3.60 (circles), and YC4.60 (squares) at pH 7.4. (*C*) pH titration curves of YC3.60 at zero and saturated Ca^{2+}.

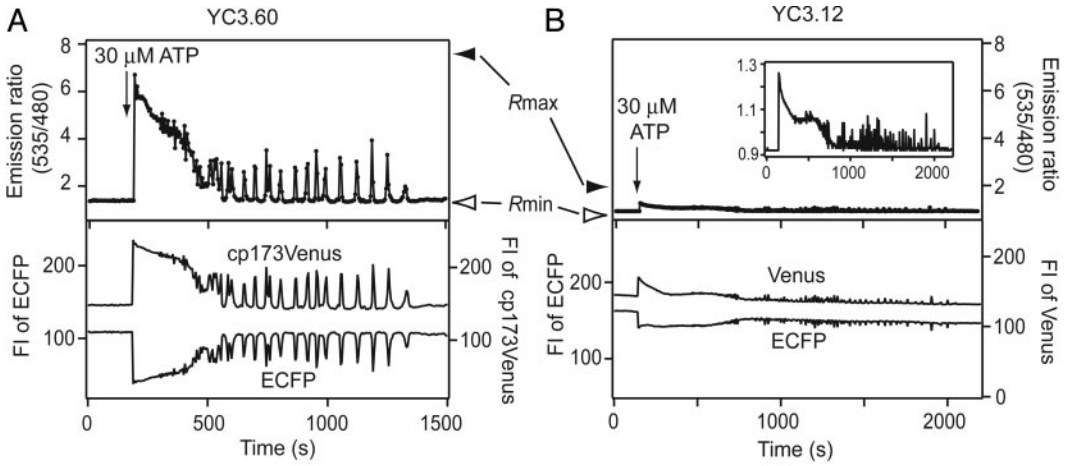

Fig. 3. Comparative measurements of Ca^{2+} dynamics in HeLa cells expressing YC3.60 and YC3.12. (*A* and *B*) Typical Ca^{2+} transients reported by YC3.60 (*A*) and YC3.12 (*B*) in HeLa cells induced with 30 μM ATP. (*Upper*) Changes in emission ratios (535/480 nm) with R_{max} and R_{min} values (indicated by solid and open arrowheads, respectively). (*B Inset*) The same graph with the ordinate expanded. (*Lower*) Changes in fluorescence intensities of CFP and cp173Venus (*A*), and CFP and Venus (*B*). The sampling interval was 5 s.

This comparison also indicates a difference in Ca^{2+} affinity between the two YCs; $K'_d = 0.25$ μM for YC3.60 vs. 1.5 μM for YC3.12. Despite the large responses, both the R_{max} and R_{min} values of YC3.60 did not vary among HeLa cells in five experiments conducted with the same microscopic system (R_{max}, 8.06 ± 0.16, $n = 12$; R_{min}, 1.37 ± 0.10, $n = 12$). Similar cell-to-cell variation was seen in the corresponding values for YC3.12 (R_{max}, 1.69 ± 0.19, $n = 14$; R_{min}, 0.89 ± 0.12, $n = 11$).

The large dynamic range and brightness of YC3.60 enable substantial improvement in both temporal and spatial resolution of $[Ca^{2+}]_c$ imaging. For fast and simultaneous acquisition of the YFP and CFP images, a color camera composed of three CCD chips (RGB: red, green, and blue) and a prism was used. For ratiometric imaging, the YFP and CFP images were captured by the G and B chips, respectively. Also, to improve spatial resolution along the *z* axis, a spinning disk unit was placed in front of the camera. A confocal real-color image of YC3.60-expressing HeLa cells is shown in Fig. 4*B*. The fluorescence was uniformly distributed in the cytosolic compartment but excluded from the mitochondria as well as the nucleus. A series of ratio images in pseudocolor acquired at video rate (Fig. 4*A* and Movie 1, which is published as supporting information on the PNAS web site) show how the increase in $[Ca^{2+}]_c$ appeared and propagated within the individual cells after stimulation with histamine. The propagation velocity was calculated to be 30 μm/s from the time courses of $[Ca^{2+}]_c$ at six aligned regions of interest in one cell (Fig. 4 *B* and *C*).

To demonstrate the benefits of YC3.60, we targeted it to the plasma membrane by fusing the membrane anchor sequence of Ki-Ras to the C terminus of the indicator ($YC3.60_{pm}$). By using similar membrane-targeting approaches, conventional YCs have not been able to monitor the Ca^{2+} dynamics beneath the plasma membrane. The fluorescence of $YC3.60_{pm}$ was distributed to the periphery and filopodial structures (Fig. 4*D*). The free Ca^{2+} concentration beneath the plasma membrane ($[Ca^{2+}]_{pm}$) was measured quantitatively (Fig. 4*E* and Movie 2, which is published as supporting information on the PNAS web site). Interestingly, $[Ca^{2+}]_{pm}$ before the application of histamine was slightly higher than the basal level of $[Ca^{2+}]_c$, which may support the notion that there exist microdomains of high $[Ca^{2+}]$ in the submicroscopic environment (10). Similar changes in $[Ca^{2+}]_{pm}$ were also observed in the filopodial structures (Fig. 4*F*).

To address whether YC3.60 could work in living organisms, we raised transgenic mice expressing $YC3.60_{pm}$. When illuminated at 480 nm, the brain of a generated line emitted bright fluorescence (Fig. 5*A Lower*) whereas that of a WT mouse produced only faint autofluorescence (Fig. 5*A Upper*). Fig. 5*B* shows a microscopic fluorescence image of area CA1 from the transgenic line. Localization of the fluorescence to the white matter as well as the rim of neurons indicates the correct targeting of $YC3.60_{pm}$. Tetanus-induced changes in electrophysiological and optical signals were simultaneously analyzed in a hippocampal slice (Fig. 5*C*). Upon tetanic stimulation of the Schaffer collateral/commissural pathway ($t = 300–600$ ms), there was a transient change in the field excitatory postsynaptic potential, which returned to a previous resting value ≈500 ms after the stimulation was over (Fig. 5*E*). In the same slice sample, fast Ca^{2+} dynamics were imaged at 100 Hz by measuring the intensity of sensitized emission from YFP (Fig. 5*D*). Averaged time courses in the signal in areas CA1 and DG are shown in Fig. 5 *F* and *G*, respectively. Upon the stimulation, a significant increase in FRET signal ($[Ca^{2+}]$) was evoked in area CA1, which was temporally broader than the change in the field potential signal measured in the same region (Fig. 5*F*). In contrast to area CA1, area DG gave a change in $[Ca^{2+}]$ oscillating at 3Hz (Fig. 5*G*), which probably reflects the θ rhythm induced by the electrical stimulation. These Ca^{2+} responses were never observed in hippocampal slices from WT mice (Fig. 5*H*).

Discussion

Cameleons or YCs have been expected to work for investigating ensemble activity of neural circuitry in living animals. Whereas the original and improved YCs display robust Ca^{2+} responses *in vitro* and in transiently transfected cell samples, their dynamic range is significantly reduced *in vivo* in the nervous systems of transgenic animals; in particular, no reliable Ca^{2+} measurements have been achieved in the brain of transgenic mice. Compared with the latest improved version of YC (YC3.12), YC3.60 is equally bright but shows 5- to 6-fold larger dynamic range. Thus, YC3.60 gives a greatly enhanced signal-to-noise ratio, thereby enabling Ca^{2+} imaging experiments that were not possible with conventional YCs. In the present study, for example, YC3.60 was targeted to the plasma membrane of HeLa cells and successfully reported $[Ca^{2+}]$ changes beneath the membrane of filopodial structures.

To address the aforementioned *in vivo* limitations of conventional YCs, furthermore, transgenic mice producing $YC3.60_{pm}$ have been constructed. The performance of $YC3.60_{pm}$ was

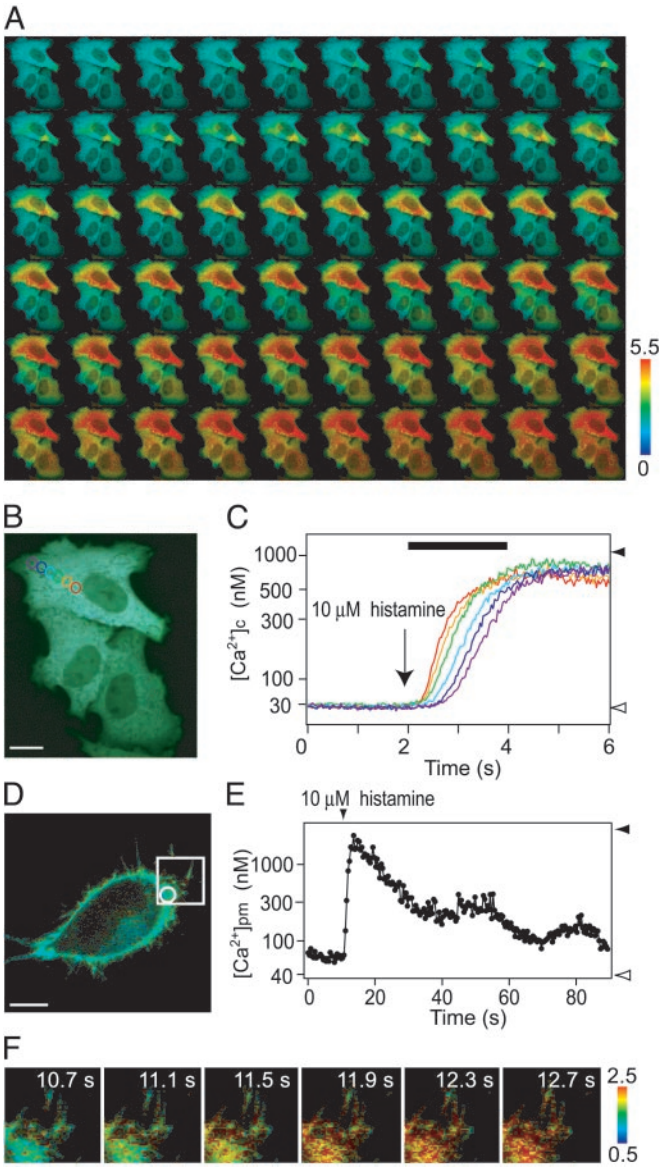

Fig. 4. Confocal Ca^{2+} imaging in cytosol and beneath the plasma membrane by using YC3.60 and YC3.60$_{pm}$, respectively. (*A*) A series of confocal pseudocolored ratio images showing propagation of $[Ca^{2+}]_c$. These images were taken at video rate. (*B*) A real-color image of the HeLa cells. In the top cell, six regions of interest (ROIs) were placed for measuring the propagation speed. (Scale bar = 10 μm.) (*C*) Time courses of changes in $[Ca^{2+}]_c$ in the six ROIs indicated in *B*. R_{max} and R_{min} are indicated by a solid and an open arrowhead, respectively. The left-hand ordinate calibrates $[Ca^{2+}]_c$ in nM. A black horizontal bar indicates the time during which the ratio images are shown in *A*. (*D*) A real-color image of a HeLa cell expressing YC3.60$_{pm}$. (Scale bar = 5 μm.) (*E*) The histamine-induced change in $[Ca^{2+}]_{pm}$ in the peripheral region indicated by a circle in *D*. R_{max} and R_{min} are indicated by a solid and an open arrowhead, respectively. The left-hand ordinate calibrates $[Ca^{2+}]_{pm}$ in nM. (*F*) A series of confocal pseudocolored ratio images showing changes in $[Ca^{2+}]_{pm}$ in filopodial structures.

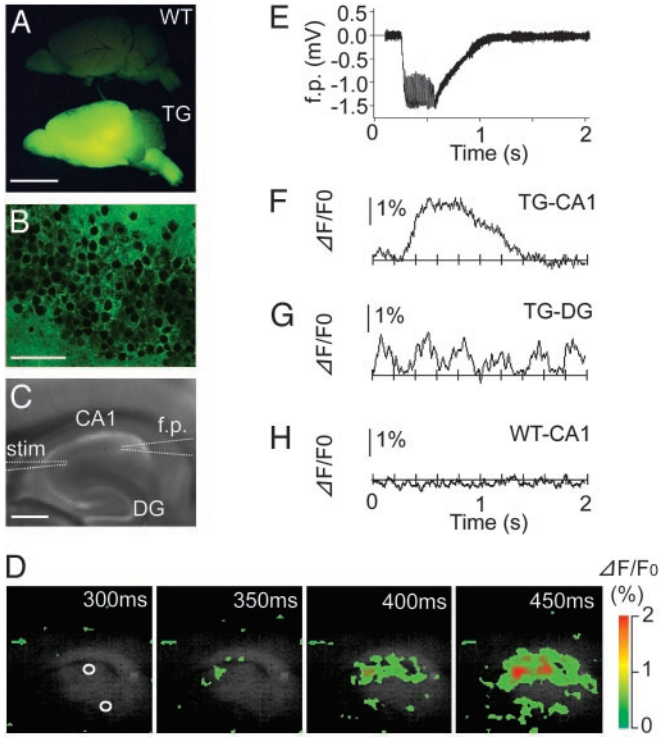

Fig. 5. Fast Ca^{2+} imaging of a hippocampal brain slice from a YC3.60$_{pm}$-producing transgenic mouse. (*A*) A low-magnification image of brains of a WT mouse and a transgenic line (no. 62) (TG). A 480DF30 excitation filter and a 535AF25 emission filter were used. (Scale bar = 0.5 mm.) (*B*) A high-magnification fluorescence image in the CA1 region of the transgenic mouse. (Scale bar = 50 μm.) (*C*) A bright-field image of hippocampal slice. Electrodes for stimulation (stim) and field recording (f.p.) are described by broken lines. (Scale bar = 0.2 mm). (*D*) A series of pseudocolored images showing a Ca^{2+} transient. The number in each image shows the time after the start of imaging. Two regions of interest were selected within regions CA1 and DG. (*E*) The field potential (f.p.) change induced by tetanus. (*F*) The time course of $[Ca^{2+}]_{pm}$ observed in area CA1 of the transgenic line. (*G*) The time course of $[Ca^{2+}]_{pm}$ observed in area DG of the transgenic line. (*H*) The time course of $[Ca^{2+}]_{pm}$ observed in area CA1 of a WT mouse. (*E–H*) Averaged traces from eight challenges.

examined by using hippocampal slices where neural activities are well characterized. To follow fast $[Ca^{2+}]_{pm}$ dynamics, we used a CCD-based digital high-speed camera (MiCAM01, Brainvision) (11), which was designed for optical imaging of neural activities with a voltage-sensitive dye. With tetanic stimulation of the Schaffer collateral/commissural pathway, we observed $[Ca^{2+}]_{pm}$ transients (≈1-s duration) and θ oscillations in regions CA1 and DG, respectively. The tetanus-induced signals were observed reproducibly and were specific to the transgenic line. However, we seemed to encounter a problem in using CaM-based genetic sensors: a reduced dynamic range when expressed in the central nervous system of transgenic animals. Because YC3.60$_{pm}$ was expressed in all cell types, the neuronal signals could be diluted by the signals from glial cells, which represent a large fraction of the total membrane of the brain. Alternatively, YC3.60$_{pm}$ might be significantly deteriorated by the interference with CaM and/or CaM-binding proteins, which are abundant in neuronal tissues.

Baird *et al.* (6), who first reported the construction of a cpGFP, attempted to improve the dynamic range of YCs by replacing the donor CFP with a cpCFP, which has a new N terminus at Tyr-145. Despite the fact that the replacement reduced the Ca^{2+}-dependent emission ratio change to only 15%, the authors believed that this single failure did not demonstrate a fundamental inefficiency of the general strategy of using circularly permuted fluorescent proteins in YCs (6). We improved on this approach by testing multiple cpYFPs as the acceptor. cp49Venus, cp157Venus, cp173Venus, cp195Venus, and cp229Venus were generated from Venus, a bright version of YFP (5). All of the three cpVenus proteins matured efficiently, probably because they all include F46L, the mutation that facilitates greatly the oxidation reaction for chromophore syn-

thesis (5), and because their N termini occur at surface-exposed loop regions of the β-barrel. In fact, the rate of fluorescence development of cpGFP depends on the position of the new N and C termini (7).

It is interesting that, among the five cpVenus proteins tested here, only cp173Venus imparts a substantial improvement in Ca^{2+}-dependent FRET. FRET is highly sensitive to the relative orientation of as well as distance between the two chromophores (12). Although we first suspected a parallel alignment of the two transition dipoles in the Ca^{2+}-bound YC3.60, our steady-state polarization measurements revealed that the Ca^{2+}-bound YC3.60 exhibited negative anisotropy. Direct visualization of the three-dimensional structure of the Ca^{2+}-bound YC3.60 by crystallographic studies will give us the structural basis of the FRET between CFP and cp173Venus. It is also possible that Venus and cp173Venus interact with the Ca^{2+}-sensing domain differently because YC2.60, YC3.60, and YC4.60 display higher affinities for Ca^{2+} than do their respective parent proteins YC2, YC3, and YC4. Single-molecule detection and spectroscopy will elucidate the mechanism of the interconversion between different conformations of CaM in the new YCs.

The process by which YC3.60 was conceived is a model for the development of GFP-based indicators. Again, the lack of improvement seen in the cp49Venus-, cp157Venus-, cp195Venus-, or cp229Venus-containing YC complexes does not necessarily indicate an inherent superiority of cp173Venus to these other cpVenus proteins. An increasing number of fluorescent indicators have been developed based on FRET between CFP and YFP (13), in which the relative position between the two chromophores of CFP and YFP is varied. Thus, the cpVenus to be used in combination with CFP should be optimized for each specific application. Also, its combined use with cpCFPs will increase further the variation of the relative position of the two transition dipoles between donor and acceptor. Because cpGFP-based indicators for Ca^{2+} were developed a few years ago (14, 15), cpGFPs themselves have been expected to become powerful tools comparable with pairs of GFP variants for FRET. Moreover, our present study may bring about an innovation in GFP technology through the marriage of circular permutation and FRET techniques.

We thank Yoko Tominaga and Chitoshi Itakura for assistance and encouragement and Katsuya Kominami for valuable advice. This work was partially supported by grants from Precursory Research for Embryonic Science and Technology (PRESTO) of the Japan Science and Technology Agency (JST) (to T.N.); Core Research for Evolution Science and Technology (CREST) of JST; the Japanese Ministry of Education, Science, and Technology; the Bio Design Program of the Ministry of Agriculture, Forestry, and Fisheries of Japan; and the Human Frontier Science Program (HFSP) (to A.M.).

1. Miyawaki, A., Llopis, J., Heim, R., McCaffery, J. M., Adams, J. A., Ikura, M. & Tsien, R. Y. (1997) *Nature* **388,** 882–887.
2. Tsien, R. Y. (1998) *Annu. Rev. Biochem.* **67,** 509–544.
3. Miyawaki, A., Griesbeck, O., Heim, R. & Tsien, R. Y. (1999) *Proc. Natl. Acad. Sci. USA* **96,** 2135–2140.
4. Griesbeck, O., Baird, G. S., Campbell, R. E., Zacharias, D. A. & Tsien, R. Y. (2001) *J. Biol. Chem.* **276,** 29188–29194.
5. Nagai, T., Ibata, K., Park, E. S., Kubota, M., Mikoshiba, K. & Miyawaki, A. (2002) *Nat. Biotechnol.* **20,** 87–90.
6. Baird, G. S., Zacharias, D. A. & Tsien, R. Y. (1999) *Proc. Natl. Acad. Sci. USA* **96,** 11241–11246.
7. Topell, S., Hennecke, J. & Glockshuber, R. (1999) *FEBS Lett.* **457,** 283–289.
8. Niwa, H., Yamamura, K. & Miyazaki, J. (1991) *Gene* **108,** 193–199.
9. Porumb, T., Yau, P., Harvey, T. S. & Ikura, M. (1994) *Protein Eng.* **7,** 109–115.
10. Marsault, R., Murgia, M., Pozzan, T. & Rizzuto, R. (1997) *EMBO J.* **16,** 1575–1581.
11. Tominaga, T., Tominaga, Y., Yamada, H., Matsumoto, G. & Ichikawa, M. (2000) *J. Neurosci. Methods* **102,** 11–23.
12. Tsien, R. Y., Bacskai, B. J. & Adams, S. R. (1993) *Trends Cell Biol.* **3,** 242–245.
13. Miyawaki, A. (2003) *Dev. Cell* **4,** 295–305.
14. Nakai, J., Ohkura, M. & Imoto, K. (2001) *Nat. Biotechnol.* **19,** 137–141.
15. Nagai, T., Sawano, A., Park, E. S. & Miyawaki, A. (2001) *Proc. Natl. Acad. Sci. USA* **98,** 3197–3202.